Electronic Supplementary Material (ESI) for Catalysis Science & Technology.

Supporting Information

Stability of Pd Nanoparticles on Carbon-Coated Supports under Hydrothermal Conditions

*Jiajie Huo,[ab] Robert L. Johnson,[ab] Pu Duan,[bc] Hien N. Pham,[bd] Deyny Mendivelso-Perez,[e] Emily A. Smith,[e] Abhaya K. Datye,[bd] Klaus Schmidt-Rohr[bc] and Brent H. Shanks[ab]**

[a]Department of Chemical and Biological Engineering and Center, Iowa State University, Ames, Iowa 50011, United States

[b]Center for Biorenewable Chemicals, Iowa State University, Ames, Iowa 50011, United States

[c]Department of Chemistry, Brandeis University, Waltham, Massachusetts 02453, United States

[d]Department of Chemical and Biological Engineering and Center for Microengineered Materials, University of New Mexico, Albuquerque, New Mexico 87131, United States

[e]The Ames Laboratory, U.S. Department of Energy, and Department of Chemistry, Iowa State University, Ames, Iowa 50011, United States

* E-mail: bshanks@iastate.edu Phone: +1 (515) 294-1895.

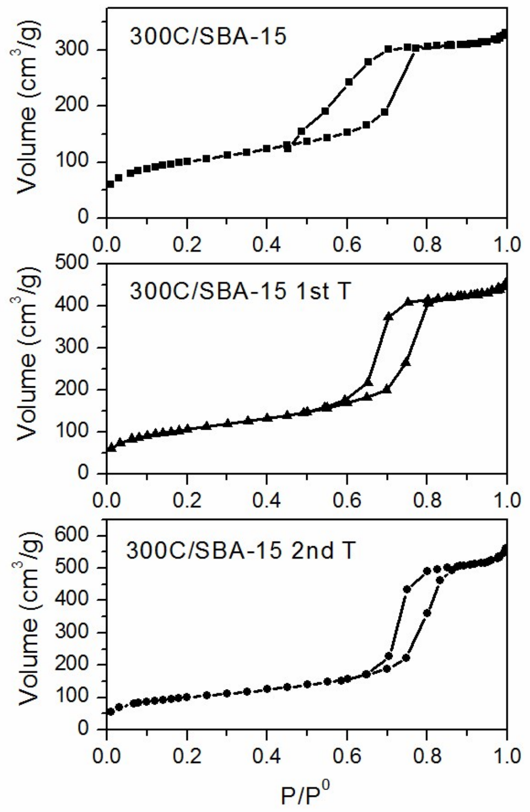

Fig. S1. Nitrogen isotherms of 300C/SBA-15 before and after hydrothermal treatment (T stands for hydrothermal treatments).

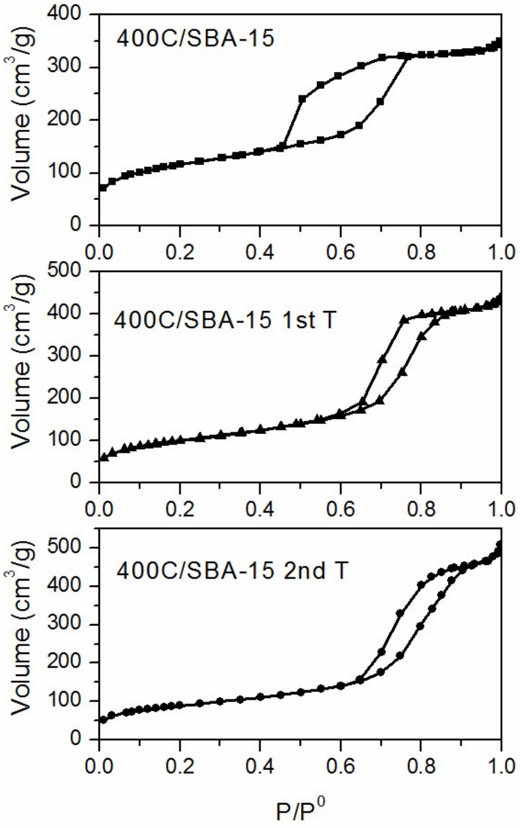

Fig. S2. Nitrogen isotherms of 400C/SBA-15 before and after hydrothermal treatment.

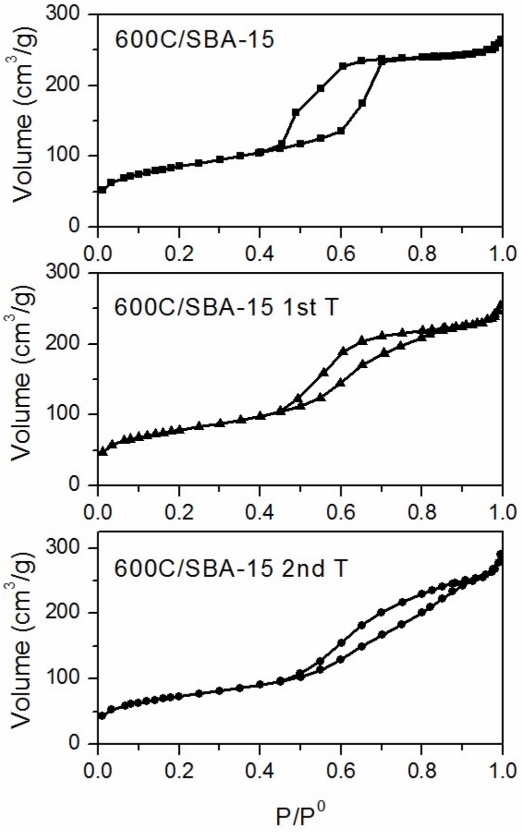

Fig. S3. Nitrogen isotherms of 600C/SBA-15 before and after hydrothermal treatment.

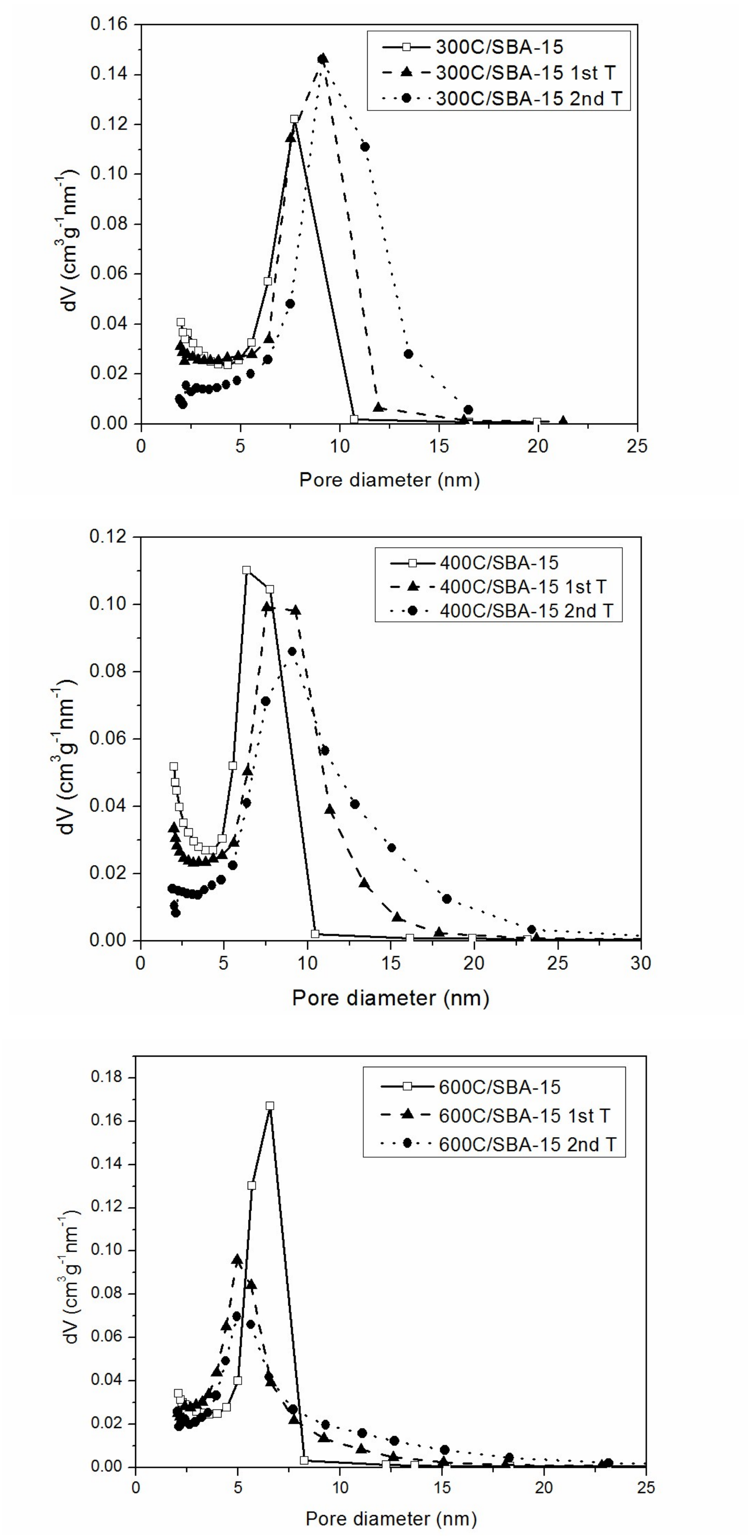

Fig. S4. Pore size distribution of Pd 300, 400, 600C/SBA15 before and after hydrothermal treatment.

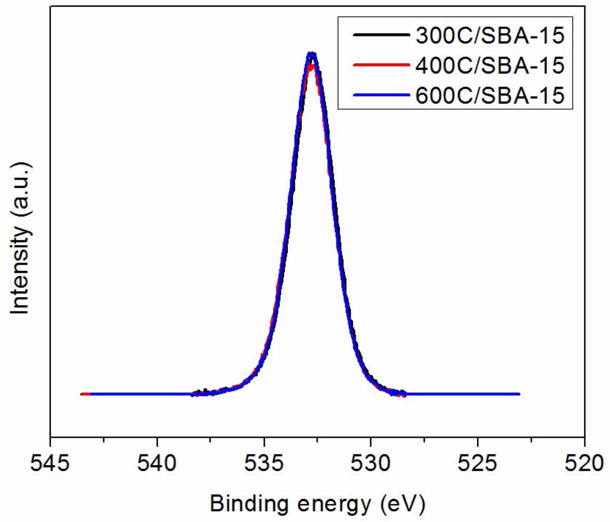

Fig. S5. XPS O1s spectra of 300C/SBA-15, 400C/SBA-15 and 600C/SBA-15

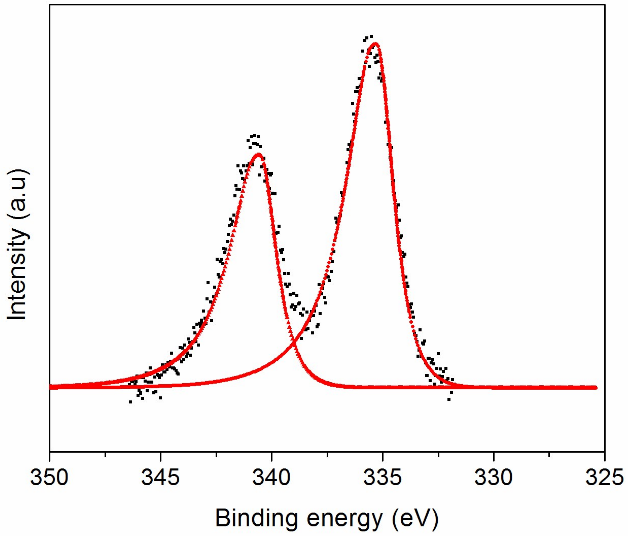

Fig. S6. XPS Pd 3d spectrum of 5%Pd 300C/SBA-15.

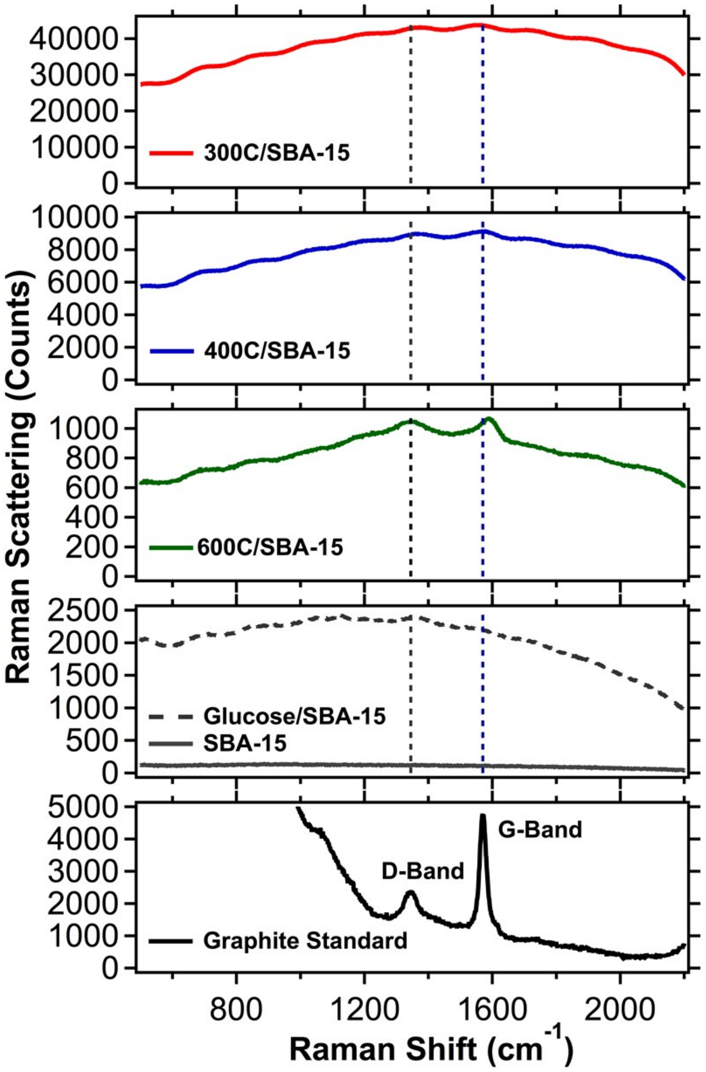

Fig. S7. Raman spectra of graphite standard, SBA-15, Glucose-SBA-15, 300C/SBA-15, 400C/SBA-15 and 600C/SBA-15.

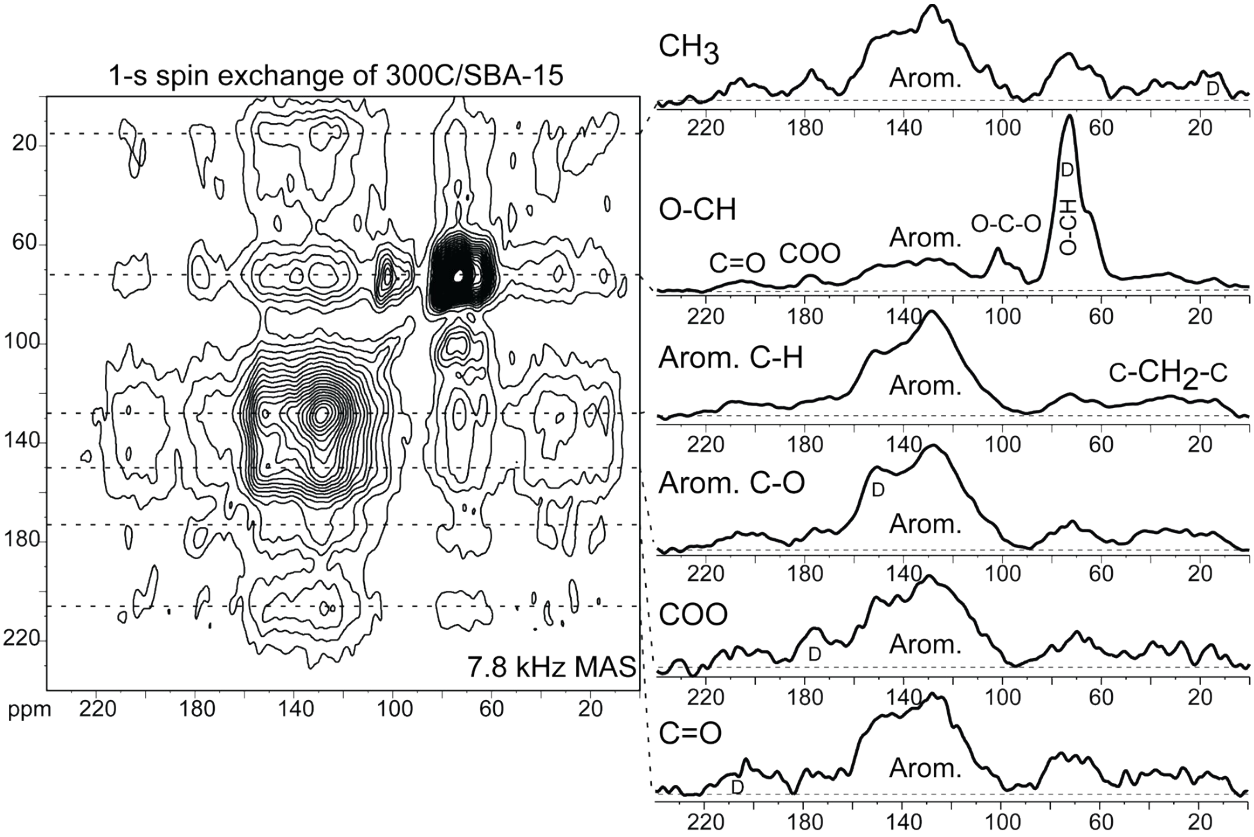

Fig. S8. Two-dimensional ^{13}C-^{13}C NMR spectrum of 300C/SBA-15 with 1-s spin exchange, measured at 7.8 kHz MAS with TOSS-deTOSS around the evolution time, and total suppression of spinning sidebands (TOSS) before detection. The horizontal cross sections corresponding to magnetization originating from various different functional groups are shown on the right. Most cross sections have the same spectral pattern, indicating equilibration of magnetization over all types of functional groups, except for the OCH cross section, which shows more pronounced cross peaks typically observed within a sugar ring.

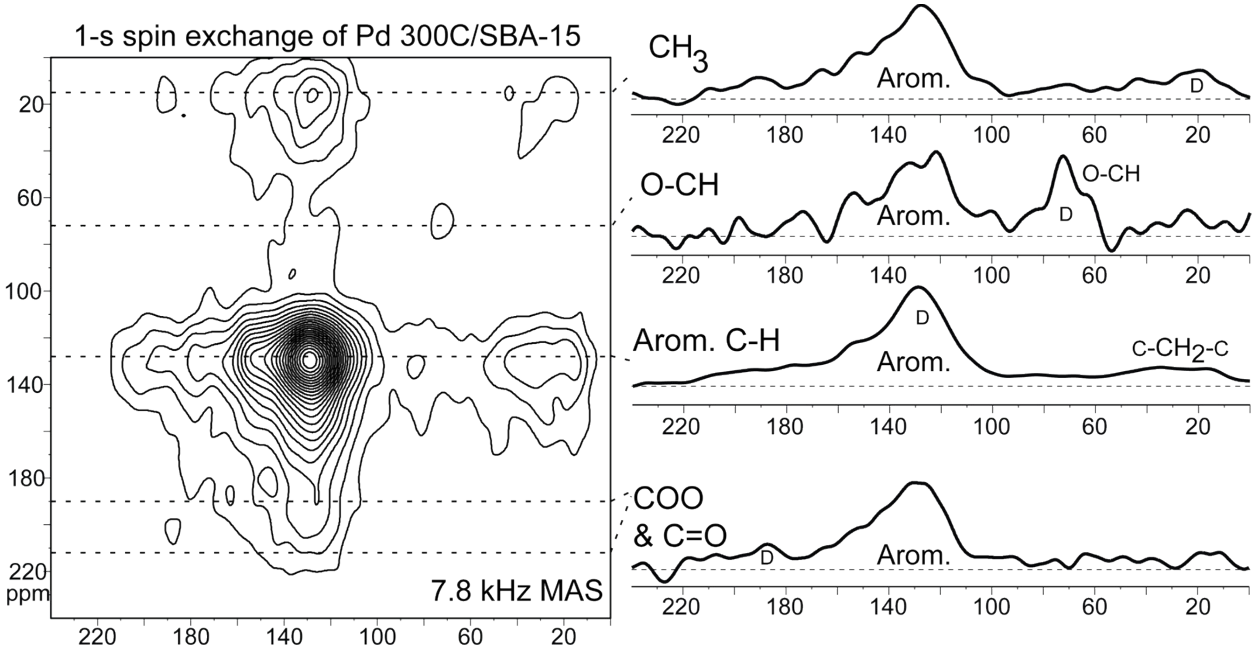

Fig. S9. 1-s ^{13}C-^{13}C spin exchange NMR spectrum of Pd 300C/SBA-15 with conditions as described in the preceding Fig. caption. The horizontal cross sections corresponding to magnetization originating from four different functional groups are shown on the right. Residual diagonal peaks are labeled by "D".

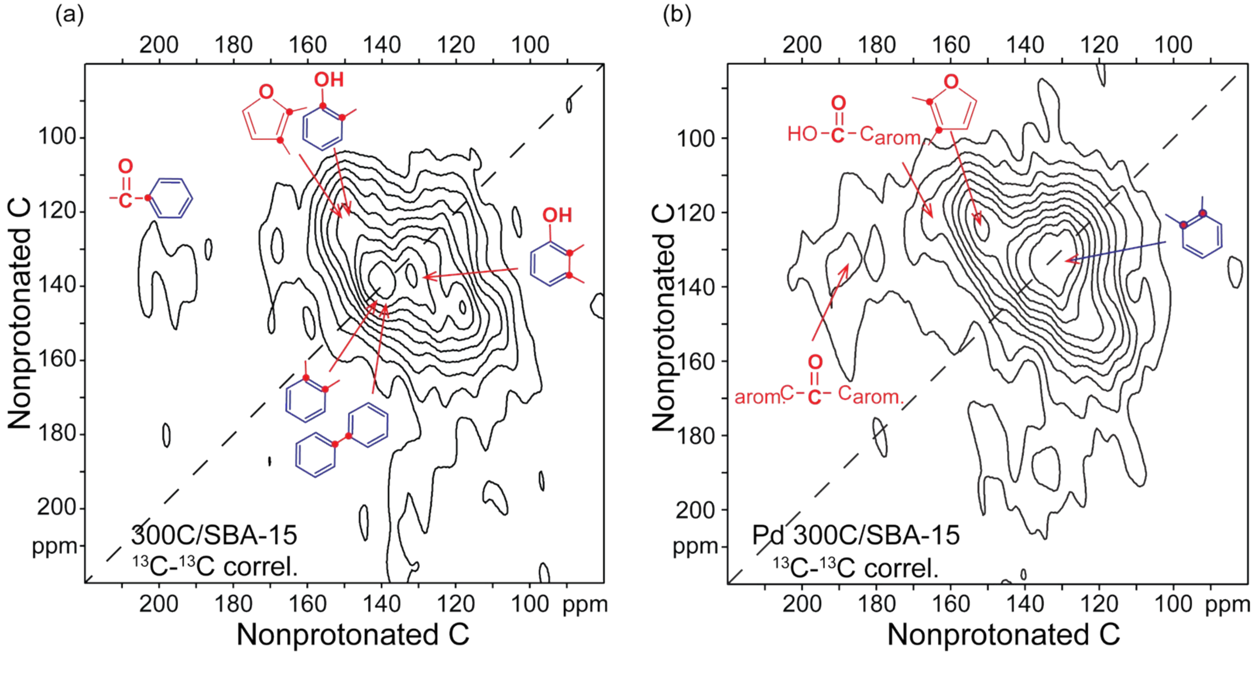

Fig. S10. 2D ^{13}C-^{13}C NMR spectra of (a) 300C/SBA-15 and (b) Pd 300C/SBA-15. These dipolar-dephased double-quantum/single-quantum correlation spectra (DQ/SQ spectra, sheared along the vertical dimension) show only correlations between directly bonded nonprotonated carbons. Some peak assignments are indicated in red and blue.

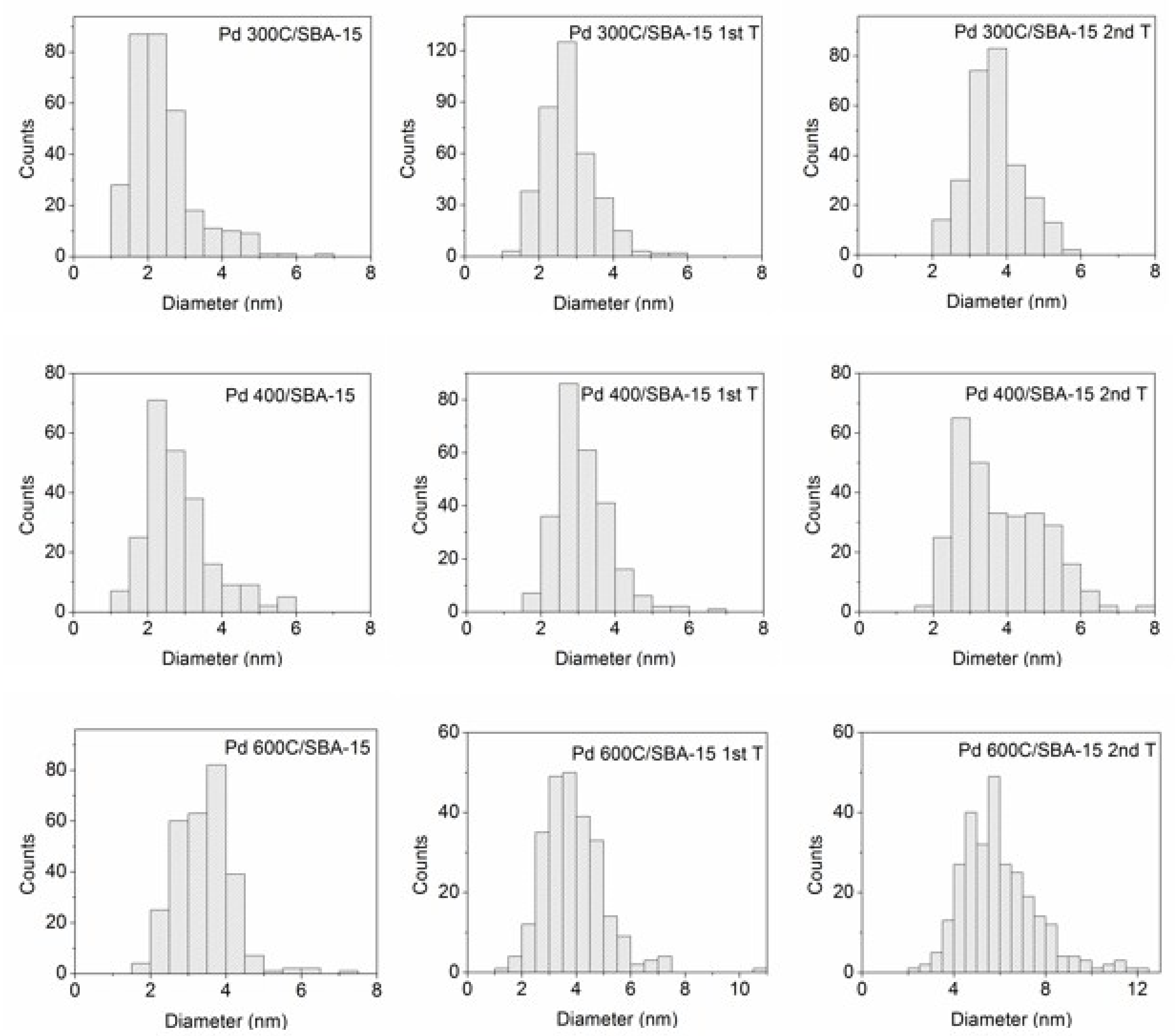

Fig. S11. Particle size distribution of Pd 300C/SBA-15, Pd 400C/SBA-15, and Pd600C/SBA15 before and after two hydrothermal treatments. The Pd particle sizes were measured from HAADF-STEM images. T stands for hydrothermal treatment.

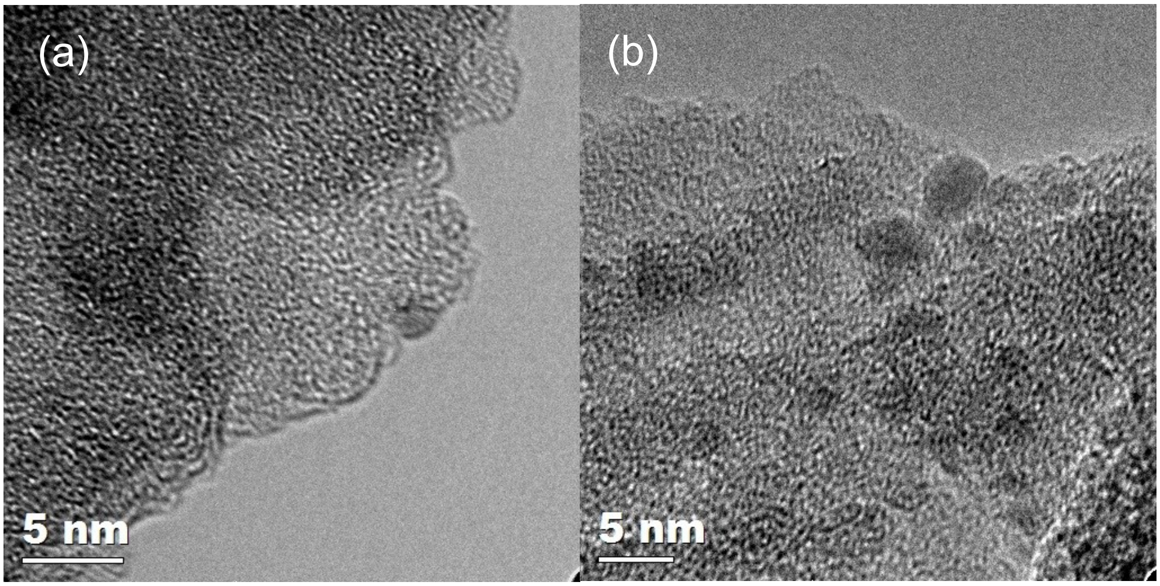

Fig. S12. HRTEM images of fresh Pd 300C/SBA-15.

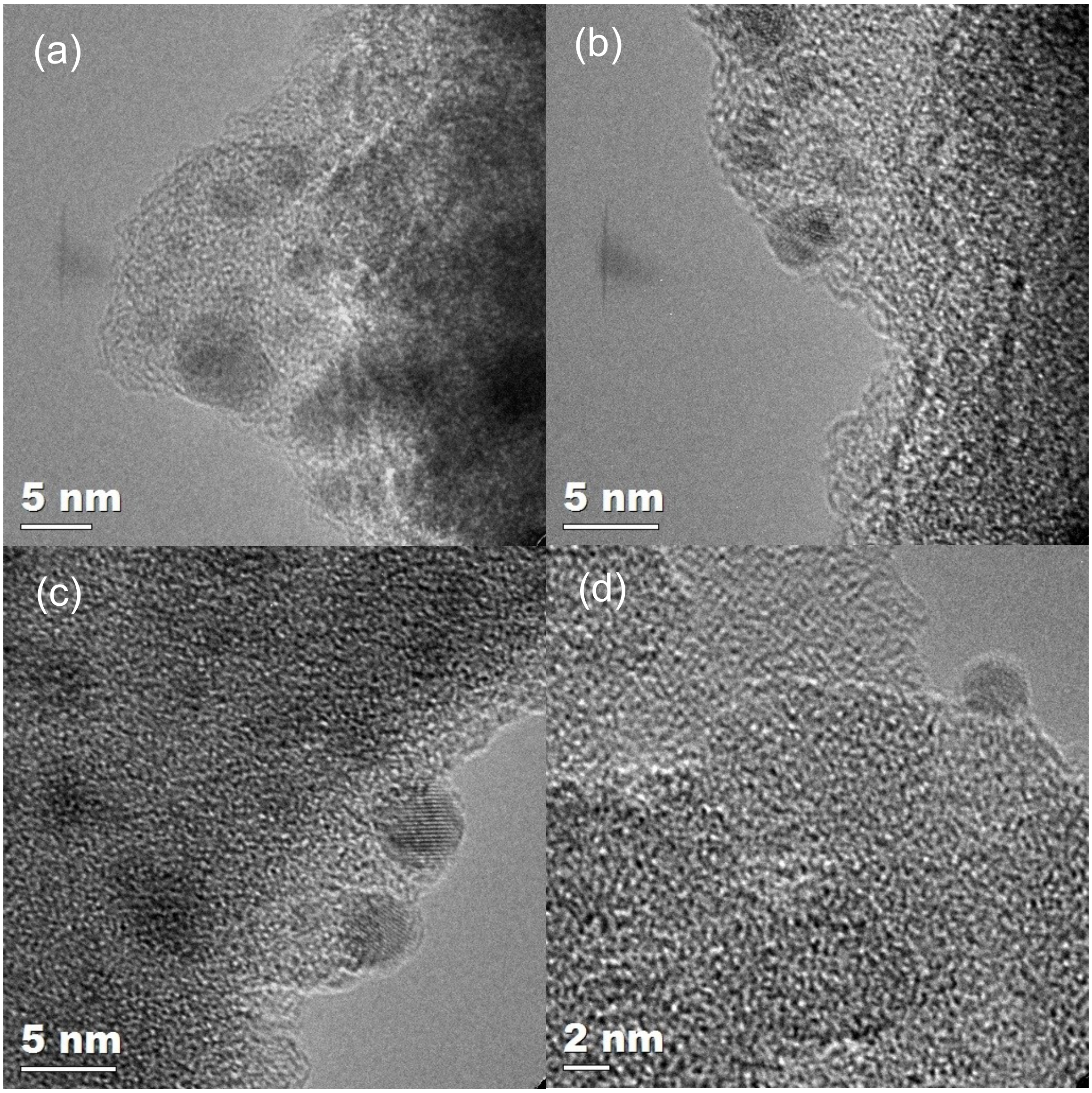

Fig. S13. HRTEM images of Pd 300C/SBA-15 after first hydrothermal treatment.

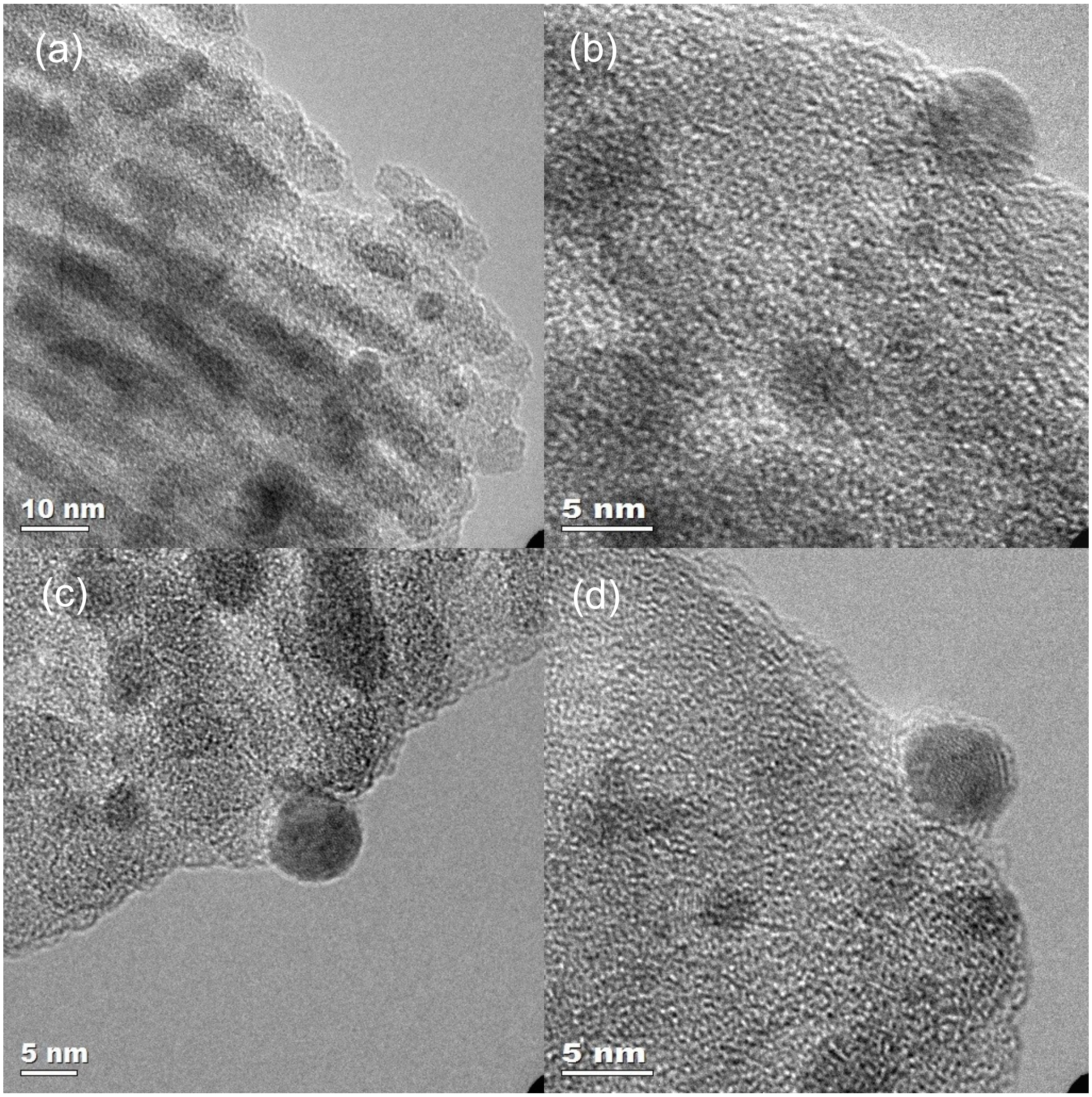

Fig. S14. HRTEM images of Pd 300C/SBA-15 after second hydrothermal treatment.

Calculation for dispersion of Pd particles

The calculation for Pd particle dispersion is based on the equation below.[1]

$$Dispersion = \frac{6M_w}{S_a \cdot d \cdot \rho \cdot N_{AV}}$$

In the equation, $M_w$is the molecular weight of Pd (106.4 g/mol); S_a is the cross sectional area of Pd atom (0.0787 nm^2); ρ is the density of Pd (12.02 g/cm^3); N_{AV} is the Avogadro's number (6.022×10^{23}); d is the surface-averaged diameter of Pd particles from STEM analysis (unit is nm). The cross sectional area of Pd atom and density value are from Micrometrics ASAP manual.[2] Putting the values generate the equation below.

$$Dispersion = \frac{1.12}{d}$$

The dispersion from CO chemisorption is calculated in the same manner.

Calculation of Weisz-Prater parameter

The Weisz-Prater parameter was used to estimate internal mass diffusion limitations using equation below

$$\Phi_i = \frac{r^{eff} \cdot r_p^2}{c_{i,s} \cdot D_{i,mix}^{eff}} < 0.3$$

Where Φ_i is the dimensionless Weisz-Prater parameter; r^{eff} is the effective rate per volume of catalyst (mol s^{-1} m^{-3}); r_p is the radium of the catalyst particle (m); $c_{i,s}$ is the concentration of reactant i at the surface of the particle (mol/m^3); and $D_{i,mix}^{eff}$ is the effective diffusivity of i in the mixture (m^2 s^{-1}). When Φ_i is less than 0.3, it is safe to ensure absence of internal mass diffusion limitations.[3]

Assuming the catalyst density is the same with carbon black XC72R as 1.7 g/cm^3 and catalyst volume is 0.6 cm^3/g. r^{eff} is calculated as 589 mol s^{-1} m^{-3}. r_p is estimated as 4 µm, same as activated carbon.[4] Diffusion coefficient of furfural and hydrogen gas in water at 80 °C is obtained as 3.361×10^{-9} m^2/s and 1.408×10^{-8} m^2/s.[5] The concentration of furfural is 0.106 M. Dissolved H_2 concentration is assumed to be the same at 100°C in water at 760 psig pressure as 0.044 M.[6]

$D_{i,mix}^{eff} = D_{i,mix} \cdot \frac{\varepsilon}{\tau}$ is used for effective diffusivity calculation of porous material. Where ε is the catalyst porosity, τ is the tortuosity. ε is assumed to be 0.9 and a value of 15 is used for τ. $D_{F,mix}^{eff}$ of furfural is calculated as 2.02×10^{-10} m^2/s. $D_{H,mix}^{eff}$ of H_2 is calculated as 8.4×10^{-10} m^2/s.

Putting the values together, Φ_F of furfural is calculated as 0.44, and Φ_H of H_2 is calculated as 0.25, both of which are near 0.3, suggesting possible internal mass transfer limitations.

Generating structural models based on quantitative and 2D ^{13}C NMR spectra

Since the quantitative 1D spectra of 400C/SBA-15 and 600C/SBA-15 showed similar characteristics as previously observed for moderate and high temperature chars,[7, 8] structural models with analogous compositions were used as the starting point. ^{13}C chemical shifts were predicted using the ACD/NMR predictor and converted into spectra with peak broadening of 15-17 ppm full width at half maximum. Spectra after dipolar dephasing were simulated by removing signals of CH and CH_2 groups, and scaling CH_3 signals by 0.57. Two spinning sidebands of 5% relative intensity each were included for the aromatic-carbon signals. The ratios of functional groups were fine-tuned to match the experimental quantitative 1D spectra, while making few changes to the connections between functional groups. For 300C/SBA-15 and Pd 300C/SBA-15, connections between functional groups identified in 2D EXPANSE and DQ/SQ spectra (Fig. 5b, 6b, and S10) were included in the structural models. The simulated structure was converted into a representative repeat unit by taking out some functional groups at the edges, and leaving out their signals. To be general, functional groups were usually taken out in pairs. For example, if a furan connected to an aliphatic chain is removed, then another aliphatic chain connected to a furan is taken out of the structure. In the end, a model with spectra of minimum difference (root mean square deviation) from the experimental spectra was chosen as representative.

The spectra of 300C/SBA-15 showed sharp carbohydrate peaks at 60-105 ppm, which matched well with the resonance positions of glucose (red vertical lines in Fig. 5a). These carbons had weak dipolar couplings to ^{1}H, since they survived after dipolar dephasing (dashed-line spectrum), indicating that these carbohydrates were highly mobile. Whether they were segregated from the pyrolyzed carbons was determined by two-dimensional ^{13}C-^{13}C exchange NMR with a long, 1-s mixing time (Fig. S8). While significant off-diagonal intensity was observed for all carbons, the O-CH cross section showed that the carbohydrates did not equilibrate their magnetization with the rest of the carbons, indicating separation on the scale of a few nanometers. Thus, the alcohol signal was mostly associated with only partially oxidized glucose somewhat separated from the rest of the carbon film. While the C-OH functionalities were not explicitly represented in our structural model in Fig. 5c, they were included in the simulation as roughly three equivalents of glucose, with COOH groups instead of CH_2OH.

References

1. C. H. Bartholomew and R. J. Farrauto, *Fundamentals of Industrial Catalytic Processes, 2nd Edition*, 2006.
2. *Micromeritics AutoChem 2920 Automated Catalyst Characterization System Operator's Manual*, V4.00 edn., 2009.
3. S. Mukherjee and M. A. Vannice, *Journal of Catalysis*, 2006, **243**, 108-130.
4. J. H. Xie, B. Huang, K. H. Yin, H. N. Pham, R. R. Unocic, A. K. Datye and R. J. Davis, *ACS Catal.*, 2016, **6**, 4206-4217.
5. C. L. Yaws, *Yaws handbook of properties of the chemical elements*, Knovel, Norwich, N.Y., 2011.
6. E. F. Stephan, N. S. Hatfield, R. S. Peoples and H. A. H. Pray, *The solubility of gases in water and in aqueous uranyl salt solutionsat elevated temperatures and pressures*, Battelle Memorial Institute, Columbus, Ohio, 1956.
7. R. L. Johnson, J. M. Anderson, B. H. Shanks, X. Fang, M. Hong and K. Schmidt-Rohr, *J. Magn. Reson.*, 2013, **234**, 112-124.
8. J. M. Anderson, R. L. Johnson, K. Schmidt-Rohr and B. H. Shanks, *Carbon*, 2014, **74**, 333-345.